Extracellular Vesicles Analysis in the COVID-19 Era: Insights on Serum Inactivation Protocols Towards Downstream Isolation and Analysis

Roberto Frigerio[1§], Angelo Musicò[1§], Marco Brucale[2], Andrea Ridolfi[2], Silvia Galbiati[3], Riccardo Vago[3], Greta Bergamaschi[1], Anna Ferretti[1], Marcella Chiari[1], Francesco Valle[2], Alessandro Gori[1#]*, Marina Cretich[1#]*

[1]: Istituto di Scienze e Tecnologie Chimiche "Giulio Natta" (SCITEC) - Consiglio Nazionale delle Ricerche
[2]: Istituto per lo Studio dei Materiali Nanostrutturati (ISMN) - Consiglio Nazionale delle Ricerche
[3]: IRCCS San Raffaele Scientific Institute, Milano, Italy

[§]: these authors equally contributed
[#]: these authors equally contributed

*: corresponding authors
alessandro.gori@cnr.it ; marina.cretich@cnr.it

Abstract

Since the outbreak of COVID-19 crisis, the handling of biological samples from known or suspected SARS-CoV-2 positive individuals demanded the use of inactivation protocols aimed at ensuring laboratory operators safety. While not standardized, these practices can be roughly divided in two categories, namely heat inactivation and solvent-detergent treatments. As such, these routine procedures should also apply to samples intended for Extracellular Vesicles (EVs) analysis. Assessing the impact of virus inactivating pre-treatments is therefore of pivotal importance, given the well-known variability introduced by different pre-analytical steps on downstream EVs isolation and analysis. Common guidelines on inactivation protocols tailored to best address EVs-specific requirements will be likely needed among the EVs community, yet deep investigations in this direction haven't been reported so far.

In the attempt of sparking interest on this highly relevant topic, we here provide preliminary insights on SARS-CoV-2 inactivation practices to be adopted prior serum EVs analysis by comparing solvent/detergent treatment vs. heat inactivation. Our analysis entailed the evaluation of EVs recovery and purity along with biochemical, biophysical and biomolecular profiling by means of Nanoparticle Tracking Analysis, Western Blotting, Atomic Force Microscopy, Transmission Electron Microscopy, miRNA content (digital droplet PCR) and tetraspanin assessment by antibody microarrays. Our data suggest an increase in ultracentrifugation (UC) recovery following heat-treatment, however accompanied by a marked enrichment in EVs-associated contaminants. On the contrary, solvent/detergent treatment is promising for small EVs (< 150nm range), yet a depletion of larger vesicular entities was detected. This work represents a first step towards the identification of optimal bio-samples inactivation protocols targeted to EVs analysis.

Introduction

The COVID-19 pandemic has forced researchers to deal with clinical specimens from known or suspected SARS-CoV-2 positive patients. Current precautionary practices demand for biological samples handling as potentially SARS-CoV-2 positive, and biocontainment guidelines to address lab operators exposure risk are adopted according to international standards and constantly updated (https://www.cdc.gov/coronavirus/2019-nCoV/lab/lab-biosafety-guidelines.html). In this regard, the minimum biosafety level to handle suspect SARS-CoV-2 specimens is BSL-2, provided that the samples have been biologically inactivated to abolish or mostly suppress virus infectivity. Common inactivation protocols are inherited from previous studies on enveloped viruses validated during the MERS or SARS outbreaks; those preceding molecular diagnostics (involving RNA extraction) are usually based on chemical treatments with detergents and chaotropic agents [1,2]. Previous experience on serology of coronaviruses also suggested treatments with a solvent-detergent combination (e.g. Triton X100/Tween 80 and tri(n-butyl) phosphate), as currently adopted for serum/plasma standards by the Medicine & Healthcare products Regulatory Agency [3]. Heat treatment is another routine inactivation method, especially for serum/plasma. On this matter, while data are still debated [1] , [4], [5] serum heat inactivation at 56°C for 30 min is emerging as a common practice.

In this scenario, arguably, it is anticipated that assessing the impact of different serum inactivation protocols on Extracellular Vesicles (EVs) isolation and analysis will be of primary relevance to the EVs community while, to the best of our knowledge, no investigation has been reported so far in this direction. EVs from biological samples are indeed tremendously complex analytes, and the well-known influence of pre-analytical practices on downstream EVs use has been driving the need for standardization and rigor criteria largely before the COVID crisis as reported in in the MISEV guidelines [6]. Given the colloidal nature of EVs and of common EVs-associated contaminants, any further pre-analytical serum treatment may indeed lead to different outcomes in terms of EVs isolation yield and purity [7] , [8].

Herein, we report on the influence of two COVID-19 serum inactivation protocols, *i.e.* solvent/detergent treatment vs. heat inactivation, on EVs recovery, purity, biophysical, biochemical and biomolecular traits. Specifically, on unbiased premises, we performed an investigation focusing on EVs isolated by ultracentrifugation (UC) from untreated (NT), heat treated (HT) and solvent/detergent (S/D) treated healthy sera, that were following analyzed by means of Nanoparticle Tracking Analysis (NTA), Western Blotting (WB), Atomic Force Microscopy (AFM), Transmission Electron Microscopy (TEM), miRNA 16-5p and miRNA 21-5p quantification by droplet digital PCR (ddPCR) and antibody microarrays for tetraspanin assessment. A flow chart of the experimental strategy is reported in Scheme 1. Our data showed that serum heat inactivation provided the highest UC recovery, yet inclusive of contaminants enrichment. Solvent/detergent treatment leads to no remarkable effect when small EVs (< 150nm range) are considered and, rather, provide the best EVs purity among the three groups. Far from being conclusive, our work aims to provide preliminary insights on viruses inactivation practices to be adopted prior serum EVs analysis, and to spark interest among the EVs-community on this highly relevant topic, that will unavoidably affect future research in the EVs field.

Results and discussion

Sample preparation

Sixteen pre-COVID serum samples from healthy donors were divided in three aliquots (750uL each). For each serum sample, one aliquot was left untreated (NT), one aliquot (HT) was set to mimic heat inactivation (56°C for 30 minutes), and one aliquot (S/D) was treated with 10mg/mL Tween 80 and 3 mg/mL tri(n-butyl) phosphate (TNBP). Hints on compatibility of such treatments with EV integrity were previously reported in studies on stability of vesicles upon different temperatures[9] and non ionic detergents [10]. The resulting 48 samples were subjected to standard ultracentrifugation (UC) at 150.000g for 2 hours. It is well documented that single-step EVs isolation procedures, including UC, are likely to lead to EVs co-isolation of contaminants such as protein aggregates, VLDLs, LDLs and chylomicrons [11] , [12], whereas a combination of sequential purification techniques may provide increased purity[13] [14]. As such, we reasoned that the simple and routinely performed EVs isolation by UC could be particularly indicative in assessing the role of serum pre-treatment on the extent of co-isolated contaminants.

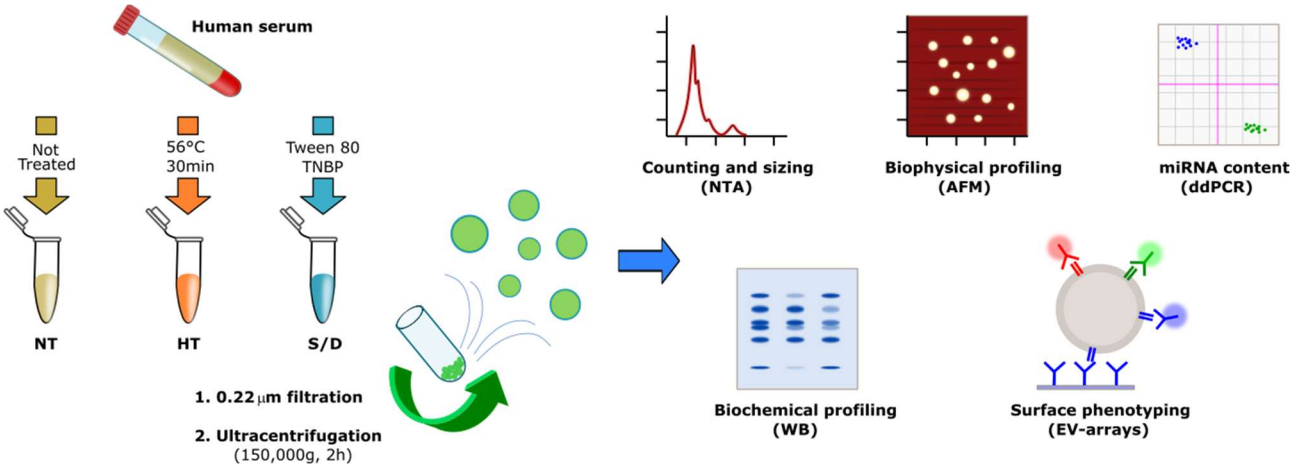

Scheme 1. Workflow describing the sample treatments, EV isolation and characterization

Nanoparticle Tracking Analysis

Pellets from UC samples were resuspended in PBS (50µL), and particle number and sizing of the 48 samples were determined by Nanoparticle Tracking Analysis (NTA) as described in Methods section. The resulting particle concentration (A), mean (B) and median (C) of particle diameter for the untreated (NT), heat treated (HT) and solvent/detergent treated (S/D) samples are shown in Figure 1.

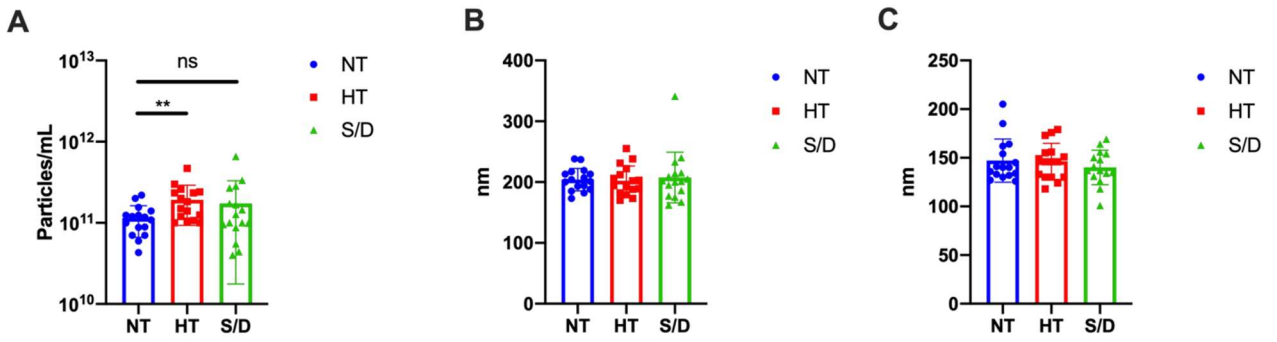

Figure 1: NTA analysis of EVs isolated by ultracentrifugation from untreated (NT), heat treated (HT) and solvent/detergent (S/D) treated healthy sera. N= 16. A: mean particle count. B: median particle size. Significative: $p<0.05$; * = $p<0.05$; ** = $p<0.01$.

In line with qualitative observation upon UC pellets recovery, NTA analysis revealed a significant ($p < 0.01$) increase in particle counting in the HT EVs compared to the NT sample, whereas no difference was detected at a statistically significant level for the S/D treated EVs (Figure 1A). Yet, the S/D samples show an higher variability in the number of UC recovered particles (Figure 1A). As for particle mean and median size, no significant differences were found among the three sample sets. It is well known that given the presence of co-isolated lipoproteins, the quantification of EVs based on particle counting by NTA tends to overestimate EV concentration[15]. Thus, we preliminary hypothesized that the increased number of recovered particles that is observed after heat-treatment could be ascribed to the increased co-precipitation of lipoproteins and other proteins aggregates triggered by heat-induced denaturation. To gain more insights on this point, Western Blotting analysis was performed

Western Blotting

Western blotting (WB) was used to confirm the presence of EV transmembrane (CD9 and CD63) and luminal proteins (Alix and TSG101) as well as the presence of common co-isolated contaminant lipoproteins by assessment of Apolipoprotein A I (Apo AI) in a set of NT, HT and S/D samples. Prior to WB, protein concentration in the pellets was assessed by Bradford assay showing an average protein content of 3.8 mg/mL both in the NT and S/D pellets whereas a remarkably higher protein concentration of 10.6 mg/mL was found in the HT sample. The samples were then appropriately diluted and loaded on the gel at the same protein amount per lane (5 ug).

Figure 2 shows the results of the WB gels for 2 representative samples for each sample group, analyzed in non-reducing conditions (A), reducing conditions (B) and the corresponding immunoblotting for the assessment of TSG101 (C), Alix (D), CD9 (F), CD 63 (G). Overall, the presence of typical EVs markers was demonstrated for all the three sample sets with similar isolation yields. However, an higher amount of contaminating Apo AI in the UC-isolated EVs is clearly detectable in the HT group (E).

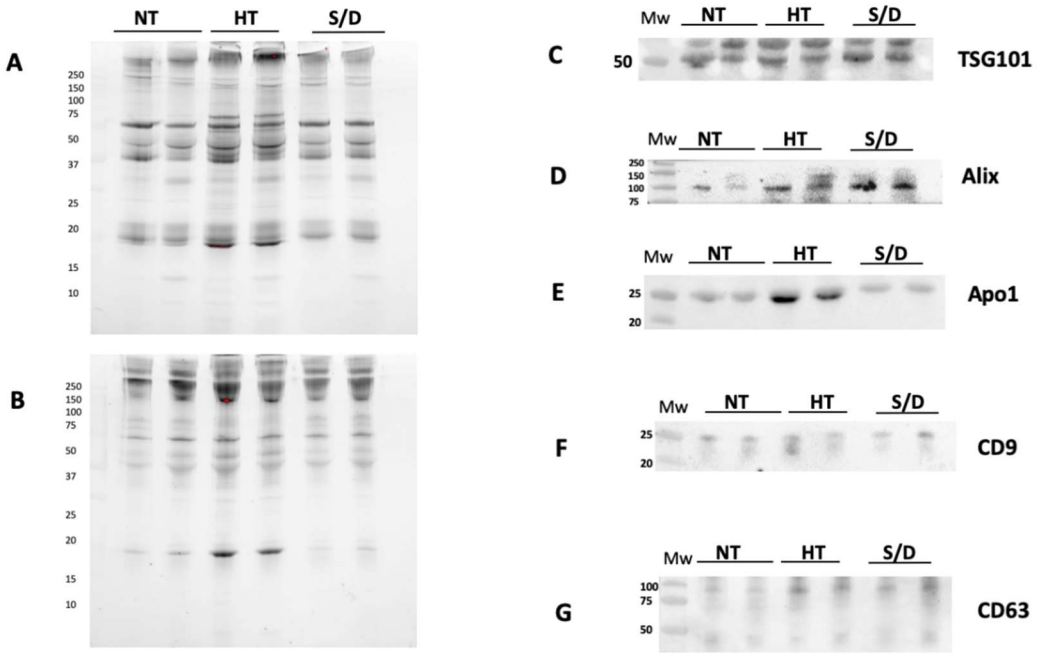

Figure 2. Western Blotting analysis of EVs isolated by ultracentrifugation (UC) from untreated (NT), heat treated (HT) and solvent/detergent (S/D) treated healthy sera. N= 12. The SDS PAGE of pellets was run in in non-reducing conditions (A) and reducing conditions (B). Immunoblotting was performed for TSG101 (C); Alix (D); contaminant Apoliprotein AI (E); tetraspanin CD9 (F) and CD63 (G).

The quantification of intensity for each immune-blotted protein band was performed and averaged. We then calculated the ratio between EV specific protein markers and the co-isolated Apo AI contaminant in order to estimate and compare the purity yield of isolated EVs after each deactivating treatment. Results are reported in Figure 3. An increase of co-isolated lipoproteins following heat treatment is clearly observable ($p < 0.01$) by comparing the ratio between TSG101 and Apo AI in the three groups. Likewise, an increase of isolation purity from lipoprotein contaminants was observable ($p < 0.001$) considering the ratio between ALIX and Apo AI. On the other hand, no evident difference among the samples is detectable for the ratio between tetraspanins CD9/CD63 and Apo AI. The selection of appropriate markers for such comparison, as a consequence, may prove extremely critical, posing multimarker selection as likely mandatory. Overall, an apparent reduction in lipoprotein contaminants is observable in the case of S/D treatment, even in comparison with untreated samples. This observation is consistent when considering all of the tested protein markers, and suggests a role of solvent/detergent in shielding those supramolecular interactions at the colloidal level among EVs and lipoproteins, that may contribute to aggregation.

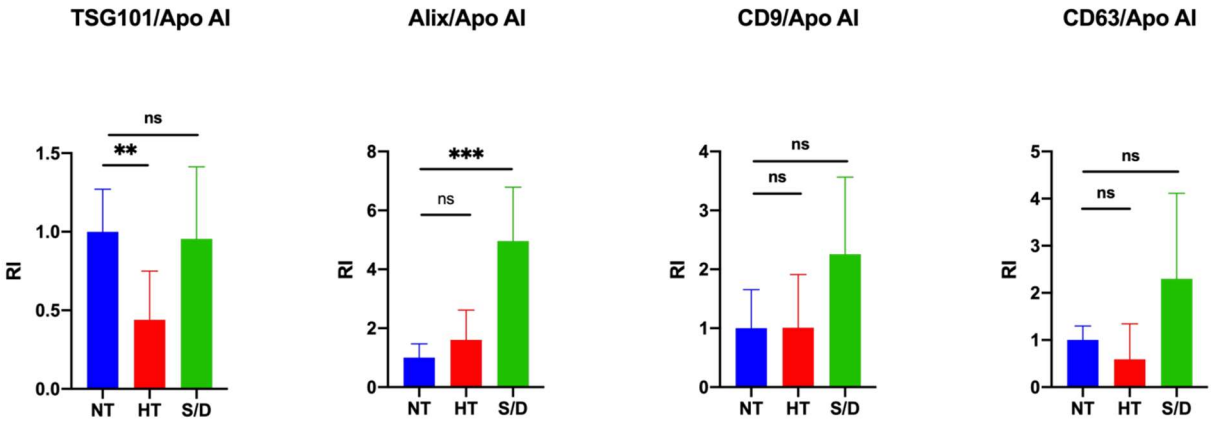

Figure 3. Quantification of blotted protein bands and ratio between EV luminal markers TSG101/Alix and EV surface markers CD9CD63 with contaminant lipoprotein Apo AI. Significative: $p<0.05$; * = $p<0.05$; ** = $p<0.01$; *** = $p<0.001$.

Atomic force microscopy (AFM) and transmission electron microscopy (TEM)

EVs collected from different serum inactivation protocols were analyzed via an high-throughput nanomechanical screening method described elsewhere[16]. Briefly, the vesicle/surface contact angle (CA) of individual EVs adsorbed on a substrate can be measured via AFM morphometry and used as a direct indication of their mechanical stiffness. The same procedure allows calculating the diameter of each observed EV prior to surface adsorption. Vesicular objects are characterized by a narrow distribution of CAs at all diameters, whereas non-vesicular contaminants show a wider dispersion of CAs [17]which can be used to infer their presence in a sample even when their globular morphology makes it difficult to discern them from EVs. Figure 4 summarizes the main differences revealed by AFM morphometric analysis across the panel of samples.

All examined EVs samples showed an abundant vesicular content (Figure 4A, left column); however, in accordance with the increased particle counting observed via NTA (Figure 1), the HT sample showed more than twice the amount of adsorbed globular objects (Figure 4B) with respect to NT and S/D samples deposited with the same procedure (see materials and methods below).

Figure 4A shows the CA vs diameter plots of around 200-300 individual EVs for each sample. All three samples were found to contain a high proportion of globular objects with diameters in the 50-100 nm range and a decidedly smaller amount of objects with diameters between 100 and 500 nm. In particular, only 2% of the EVs in the S/D sample had a diameter above 100nm (Figure 4C), with no individual S/D treated EV having a diameter >150 nm (Figure 4A, right column). In contrast, a more substantial amount of EVs in both other samples had diameters above 100nm (respectively 22% and 31% of the EVs measured in NT and HT samples, Figure 4C).

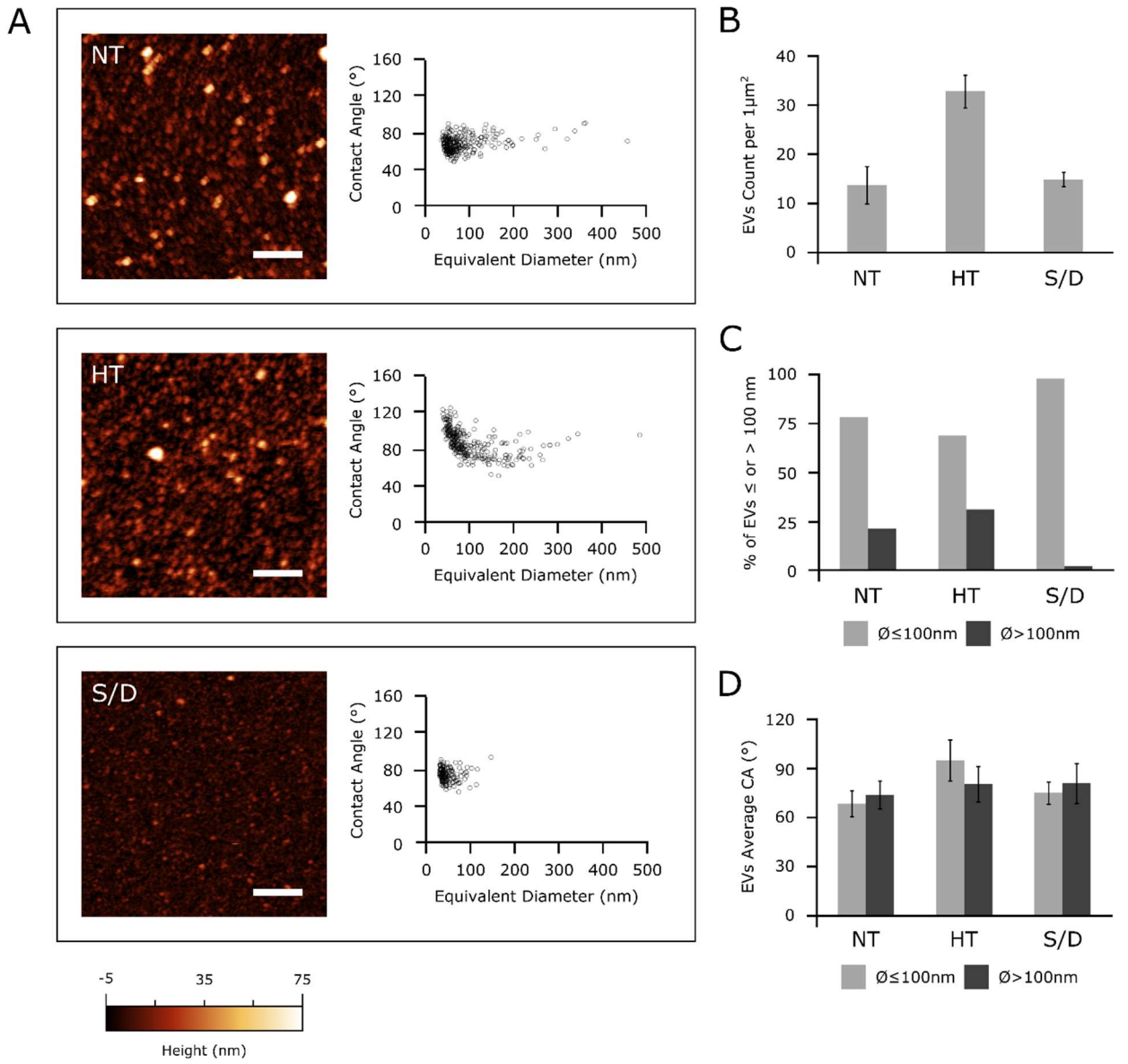

Figure 4. (A): left column – representative AFM micrographs of NT, HT and S/D samples. Scale bars are 1µm. Right column – scatterplots of surface contact angle VS diameter in solution of EVs measured via quantitative AFM morphometry as described elsewhere.[16] Each circle is an individual EV. (B): surface density of globular objects in NT, HT and S/D samples deposited with the same protocol (see materials and methods); (C) percentage of adsorbed EVs having diameters above or below 100 nm in their spherical conformation; (D) average surface/vesicle contact angle (representative of mechanical stiffness) of EVs with diameters above or below 100 nm.

Figure 4D shows the average CAs of EVs smaller and larger than 100 nm in the three samples. The NT CA/diameter scatterplot in Figure 4A does not show any significant CA discontinuity between the two ranges of diameters; accordingly, average CA values of smaller (68±8°, N=242) and larger (73±8°, N=67) EVs are similar in this sample (Figure 4D). The S/D sample shows very similar values (74±7°, N=171 for smaller and 79±12°, N=4 for larger EVs), suggesting that while the solvent/detergent treatment dramatically

reduced the amount of larger EVs, it did not significantly impact the structural integrity of the remaining EVs, which continue to show the same mechanical characteristics of untreated ones. The same consideration can be made for larger EVs in HT samples (average CA = 79±11°, N=103). In contrast, globular objects with diameters below 100nm have a significantly higher CA (94±12°, N=226) in HT, suggesting marked structural or compositional differences in this sub-population of objects with respect to other samples. This was further confirmed by TEM analysis, which highlighted the prevalence of small electron lucent lipoprotein particles [13 18] in HT samples (Figure 5b). On the other hand, particles with characteristic EVs-traits were more abundantly found in reference NT samples (Figure 5a).

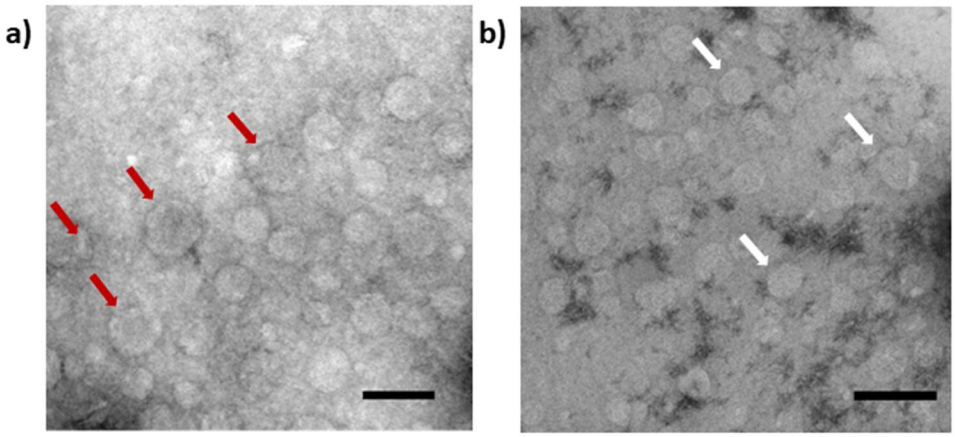

Figure 5. TEM images of a) NT samples and b) HT samples. The black bar are 100nm. Red arrows exemplifies particles with characteristic EVs traits. White arrows highlight representative lipoprotein-like particles.

Taken together, these results suggest the possibility that NT samples might contain different types of vesicular objects sharing similar mechanical characteristics but having different average dimensions, with a diameter threshold of around 100 nm separating the main subpopulations.
Although the absence of significant CA differences across all sizes in non-treated EVs makes this hypothesis only tentative, HT and S/D treatments seem to selectively act on only some of the putative subpopulations: S/D is able to deplete larger EVs, while HT enriched the solution with a population of objects with distinct mechanical properties.
To further investigate in this direction and to evaluate the impact of serum inactivation pre-treatments on the analytical outcome of techniques with clinical value potential, surface phenotyping by EVs-microarrays and digital PCR experiments to quantify selected miRNAs content were undertaken.

Microarray analysis

EVs microarrays are high-throughput analytical platforms that are used to phenotype EVs. In this technique, antibodies [19] or peptide ligands [20] are used to selectively capture EVs by their most common surface-

associated proteins or by membrane sensing, followed by fluorescence-based immune-staining to phenotype EVs subpopulations. Here, a silicon based microarray platform for enhanced fluorescence detection [21] , [22] was used in a typical EVs-array scheme, where EVs from the NT, HT and S/D groups were incubated at 10 [11] particles/mL and immune-captured by anti-tetraspanin antibodies, and then incubated with a cocktail of biotinylated anti CD9/CD63/CD81 followed by Cy3 labelled streptavidin. Figure 6 reports the resulting fluorescence intensity for each capture antibody.

As a general trend, we could detect a decrease of tetraspanin-associated immunoreactivity in the inactivated samples, which appears to be more pronounced in the case of the S/D treated samples. This may suggest partial denaturation of EVs surfaces markers, which could in turn affect either EVs capturing on the analytical surface and/or the following immune-staining step. On the other side, we can't rule out a different content in membrane-associated antigens otherwise co-isolated during UC processing, which could account for background signal and contribute to the detected differences. In addition, the high individual variability in the sample sets suggests that a cautious pondering is required before extrapolating a general behavior, and the overall picture could prove tricky to be unambiguously defined. Notwithstanding this, the overall impact of samples treatment appears to not preclude the possibility of EVs immune-phenotyping.

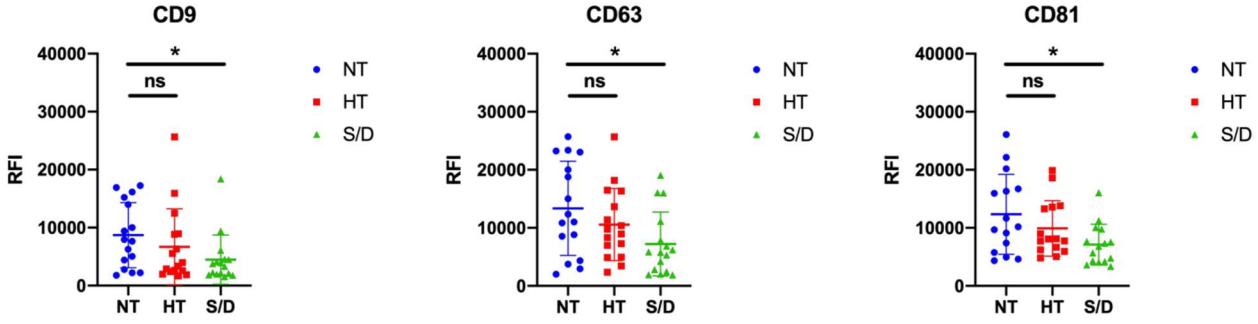

Figure 6. Results of immune-phenotyping by EV microarrays of EVs isolated by ultracentrifugation from untreated (NT), heat treated (HT) and solvent/detergent (S/D) treated healthy sera. N= 16. EVs were captured by CD9, CD63 and CD81 antibodies and fluorescently stained by a mixture of anti-CD9/CD63/CD81 antibodies. Significative: $p<0.05$; * = $p<0.05$.

miR-16-5p and miR-21-5p ddPCR analysis

The presence of various RNA molecules in EVs is well established, and their role in regulatory and pathological processes is currently matter of intensive investigation. Among different RNA classes, microRNAs (miRNA) are abundantly harbored in many body fluids via encapsulation and/or association to EVs, which avoid nucleolytic degradation, as well as transported by lipoproteins [23].

We selected two representative miRNAs, namely miR-16-5p and miR-21-5p to compare if /how serum inactivation protocols could influence the miRNA expression.

MiR-16-5p is reported in literature to be one of the most abundance miRNA in EVs [24] while miR-21-5p is reported to be associated to lipoproteins and could be involved in lipid metabolism [25]. We quantitatively detected miRNAs expression within NT, HT and S/D groups by ddPCR analysis; results are summarized in Figure 7. Data analysis highlights a clear trend for both miR-16-5p and miR-21-5p, with an increased amount detected within the heat treated samples. This observation is in accordance with the apparent higher EV isolation yield for the heat-treated sample perceivable by protein quantification and NTA. On the other hand, given the reported data on EVs purity (see WB section), that instead suggested HT samples to contain higher levels of co-isolated contaminants, a more comprehensive interpretation should take into account the reported association of RNAs also to RNA-binding proteins (RBPs) and, especially for miRNA 21-5p to high- and low-density lipoproteins [23], [26]whose content is likely to be increased in UC-recovered pellet after serum heat inactivation.

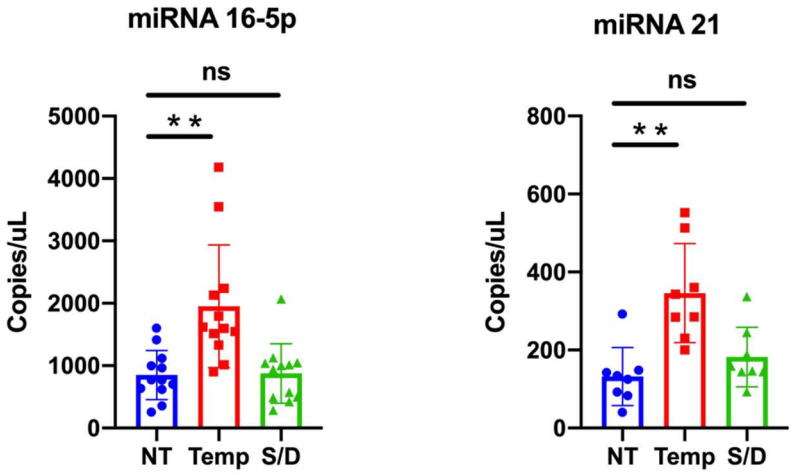

Figure 7. miR-16-5p and miR-21-5p expression levels in untreated (NT), heat treated (HT) and solvent/detergent (S/D) treated healthy sera analyzed by droplet digital PCR. Significative: $p<0.05$; * = $p<0.05$; ** = $p<0.01$.

Conclusions

Our study was aimed at introducing preliminary insights on the role of different SARS-CoV2 inactivation protocols prior to serum EVs isolation and analysis. Exacerbated by the current pandemic scenario, this topic, arguably, should be considered of more broad relevance to the EVs community. Clinical samples preparation is indeed known to have a profound impact on the isolation of EVs and related contaminants. A full awareness on the effect of any additional sample pre-analytical treatment should be consequently arisen among EVs-users, particularly due to the fact that an interlaboratory consensus on protocols for SARS-CoV2 serum inactivation protocols is far from being reached. In this sense, analytical laboratories which are collectors of EVs-samples isolated by clinicians may be particularly affected.

Far from being conclusive, our data suggest that the use of solvent/detergent addition could be seen a as a preferable virus deactivating method, taking EV's purity into account, as far as small EVs isolation and analysis are concerned. Non-ionic detergents are relatively mild and usually non-denaturing [15] , yet known to break lipid-lipid and lipid-protein interactions. This could account for the apparent higher purity of EVs obtained by this method (see WB analysis), which contrasts with the high content of lipoparticle contaminants found following heat treatment. In this sense, their standard use in UC cycles could be worth of further investigation. On the other side, solvent/detergent treatment led to the depletion of vesicular particles of larger size (>150nm), and their use should be cautiously pondered if this EVs subpopulation represents the target of analysis. In contrast, heat-based protocols provided higher recovery, and the enrichment in EVs contaminants could be counterbalanced by a subsequent step of purification. Overall, the inactivation procedure should be tailored considering the downstream analysis to be undertaken, and further work will be needed in this direction to identify the best possible practices.

Materials and methods

Reagents

Ultracentrifugation

750 ul of serum were diluted 1:1 with PBS, filtered with 0.22 mm filters (Merck Millipore) and centrifuged in a *Optima™ TLX Preparative Ultracentrifuge, Beckman CoulterTM* at 150.000 g for 120 minutes at 4°C with a *TLA-55 Rotor (Beckman CoulterTM)* to pellet EVs. After supernatant was carefully removed, EV-containing pellets were stored at -80°C until use.

Nanoparticle Tracking Analysis

Nanoparticle tracking analysis (NTA) was performed according to manufacturer's instructions using a NanoSight NS300 system (Malvern Technologies, Malvern, UK) configured with 532 nm laser. All samples were diluted in filtered PBS to a final volume of 1 ml. Ideal measurement concentrations were found by pre-testing the ideal particle per frame value (20–100 particles/frame). Following settings were adjusted according to the manufacturer's software manual. A syringe pump with constant flow injection was used and three videos of 60 s were captured and analyzed with NTA software version 3.2 . From each video, the mean, mode, and median EVs size was used to calculate samples concentration expressed in nanoparticles/mL

Protein quantification

We performed Bradford Assay to quantify protein concentration on our samples. The samples were added in a Bradford solution (BioRad Protein Assay 500-0006) 1:5 diluted in water and analysed by a spectrophotometer (Labsystem, Multiskan Ascent) at the wavelength of 595 nm. Furthermore, we analysed standard protein solutions to build a calibration line to discover the right protein concentration of our samples.

SDS-PAGE and Western blot analysis

Treated EVs were added at Laemmli buffer and boiled for 5 minutes at 95 °C. Specifically, 10 µg of EVs were prepared in non-reducing conditions for tetraspanins detection, while 10 µg were used for soluble protein detection. Proteins were separated by SDS-PAGE (4-20%, Mini-Protean TGX Precast protein gel, Bio-Rad) and transferred onto a nitrocellulose membrane (BioRad, Trans-Blot Turbo). Nonspecific sites were saturated

with a blocking solution for 1h (EveryBlot Blocking Buffer, BioRad). Membranes were incubated overnight at 4 °C with anti-CD9 (1:1000, BD Pharmingen), anti-CD63 (1:1000; BD Pharmingen,), anti-Alix (1:1000, Santa Cruz), anti-TSG101 (1:1000, Novus Bio) and anti-Apo1 (1:1000, Santa Cruz). After washing with T-TBS, membranes were incubated with the horseradish peroxidase-conjugated (Jackson ImmunoResearch) secondary antibodies diluted 1:3000 for 1 hour. After washing, the signal was detected using Bio-Rad Clarity Western ECL Substrate (Bio-Rad) and imaged using a Chemidoc XRS+ (BioRad).

AFM sample preparation, imaging and morphometry

Borosilicate glass coverslips (Menzel Gläser GmbH, Germany) were first incubated for 1h in 2:1 H_2SO_4:H_2O_2(30% v/v) solution, then rinsed with ultrapure water, subjected to 3 x 30 minutes successive sonication cycles in acetone, isopropanol and ultrapure water, and finally dried under gentle nitrogen flow. Glass slides were then exposed for 5 minutes to air plasma and functionalized with (3-Aminopropyl)triethoxysilane (APTES) in vapor phase for 2h. Resuspended EVs solutions were diluted 1:100 with ultrapure water; 5 µl aliquots of the diluted solutions were then left to adsorb on APTES-functionalized slides for 30 minutes. AFM imaging was performed in PeakForce mode on a Multimode8 AFM microscope equipped with a type JV scanner and a sealed fluid cell (Bruker, USA). Image analysis was performed as described elsewhere[16].

TEM sample preparation, microscope description

The Transmission Electron Microspopy (TEM)images were collected through a ZEISS Libra 200FE, equipped with a second generation Omega filter, HAADF detector for STEM images, and also the Energy dispersive X-ray Spectroscopy. The sample were drop on a carbon/formvar TEM grid, then blotted and treated with Uranyl less (EMS-Electron Microscopy Science) contrast agent. The detailed protocol was described elsewhere.[27]

EV array

Silicon slides (SVM, Sunnyvail, CA) were coated by MCP2 (Lucidant Polymers) as follows: slides were treated with oxygen plasma for 15 min. MCP2 was dissolved in DI water to final concentration of 2% w/v and then diluted with ammonium sulphate solution 40% at ratio 1:1. Subsequently, silicon slides were immersed into the polymer solution for 30 min, then washed with DI water, dried under nitrogen steam and cured for 15 min under vacuum at 80°C. Slides were spotted using a non-contact Spotter S12 (Scienion Co., Berlin, Germany), in each subarray we spotted anti-CD9, anti-CD63 and anti-CD-81 (Ancell) antibodies and a cocktail of the three. Each antibody was spotted with a final concentration of 1 mg/ml with 50 mM Trealose. Printed slides were placed in a humid chamber overnight at room temperature. Then they were blocked in 50 mM ethanolamine in water solution for 1 h, washed with water, and dried under a stream of nitrogen.

EVs samples were diluted with filtered PBS and incubated for 2 hours at particles concentration of 10^{10} particles/mL. Subsequently, the samples were removed and the slides were washed with washing buffer and we incubated with the secondary antibody (anti-CD9-Biotin, anti-CD63-Biotin and anti-CD81-Biotin, Ancell) diluted in ratio 1:1000 in incubation buffer 10X for 1 hour. Then, we re-incubated the slide with Streptavidin-Cy3 (Jackson ImmunoResearch) conjugated diluted in ratio 1:1000 in incubation buffer 10X for the detection for 1 hour. Finally, slides were washed and dried and the analysis were performed by TECAN power scanner 50% laser intensity and 500% gain.

miRNA isolation and retrotrascription

miRNAs were isolated from ultracentifuged EVs resuspended in 25 ul of phosphate buffered saline (PBS) using the Maxwell® RSC miRNA Plasma and Serum Kit (AS1680, Promega) following the manufacturer's instruction. The RNA was eluted in 35µl of nuclease-free water.
cDNA was obtained using the TaqMan® MicroRNA Reverse Transcription kit (ThermoFisher) combined with TaqMan MicroRNA Assays (ThermoFisher). In particular, we used 5 ul of eluted RNA and 3 ul of primers specific for human miR-16 (assay ID 000391) and miR-21 (ID 000397). The reaction was performed with an initial incubation at 16°C for 30 min and a following step at 42°C for 30 min, finally, in order to terminate the RT step, a final incubation at 85°C for 5 min was succeeded.

ddPCR reagents and cycling conditions

The miR-16-5p and miR-21-5p expression levels were performed by droplet digital PCR (ddPCR) using the QX100 ddPCR platform (Bio-Rad, Hercules, CA). The QX100 droplet generator was used to generate an emulsion of about 20,000 droplets. The volume of the PCR mix was 20 µL including 10 µL of ddPCR™ Supermix for Probes (No dUTP), 1 µL of probe (miR-16 or miR-21) and 5 ul of cDNA template. The droplet emulsion was thermally cycled on C1000 Touch Thermal Cycler (Bio-Rad) instrument. Cycling conditions were 95°C for 5 min, followed by 40 cycles of amplification (94°C for 30 s and 55°C for 1 min), ending with 98°C for 10 min, according to the manufacturer's protocol. The concentration of the target was calculated automatically by the QuantaSoft™ software version 1.7.4 (Bio-Rad).

EV-TRACK

We have submitted all relevant data of our experiments to the EV-TRACK knowledgebase (EV-TRACK ID: EV200180) (Van Deun J, et al. *EV-TRACK: transparent reporting and centralizing knowledge in extracellular vesicle research.* Nature methods. 2017;14(3):228-32)."

Acknowledgements
Work partially funded from the European Union's Horizon 2020 research and innovation programme under grant agreements No. 951768 (project MARVEL), No. 801367 (project EVfoundry), No. 952183 (project BOW), and Regione Lombardia&Fondazione Cariplo, grant n° 2018-1720 (project HYDROGEX).

References

(1) Pastorino, B.; Touret, F.; Gilles, M.; de Lamballerie, X.; Charrel, R. N. Heat Inactivation of Different Types of SARS-CoV-2 Samples: What Protocols for Biosafety, Molecular Detection and Serological Diagnostics? *Viruses* **2020**, *12* (7), 735. https://doi.org/10.3390/v12070735.

(2) Pastorino, B.; Touret, F.; Gilles, M.; Luciani, L.; de Lamballerie, X.; Charrel, R. N. Evaluation of Chemical Protocols for Inactivating SARS-CoV-2 Infectious Samples. *Viruses* **2020**, *12* (6), 624. https://doi.org/10.3390/v12060624.

(3) Darnell, M. E. R.; Taylor, D. R. Evaluation of Inactivation Methods for Severe Acute Respiratory Syndrome Coronavirus in Noncellular Blood Products. *Transfusion* **2006**. https://doi.org/10.1111/j.1537-2995.2006.00976.x.

(4) Hu, X.; Zhang, R.; An, T.; Li, Q.; Situ, B.; Ou, Z.; Wu, C.; Yang, B.; Tian, P.; Hu, Y.; Ping, B.; Wang, Q.; Zheng, L. Impact of Heat-Inactivation on the Detection of SARS-CoV-2 IgM and IgG Antibody by ELISA. *Clinica Chimica Acta* **2020**, *509*, 288–292. https://doi.org/10.1016/j.cca.2020.06.032.

(5) Hu, X.; An, T.; Situ, B.; Hu, Y.; Ou, Z.; Li, Q.; He, X.; Zhang, Y.; Tian, P.; Sun, D.; Rui, Y.; Wang, Q.; Ding, D.; Zheng, L. Heat Inactivation of Serum Interferes with the Immunoanalysis of Antibodies to SARS-CoV-2. *Journal of Clinical Laboratory Analysis* **2020**. https://doi.org/10.1002/jcla.23411.

(6) Théry, C.; Witwer, K. W.; Aikawa, E.; Alcaraz, M. J.; Anderson, J. D.; Andriantsitohaina, R.; Antoniou, A.; Arab, T.; Archer, F.; Atkin-Smith, G. K.; Ayre, D. C.; Bach, J.-M. M.; Bachurski, D.; Baharvand, H.; Balaj, L.; Baldacchino, S.; Bauer, N. N.; Baxter, A. A.; Bebawy, M.; Beckham, C.; Bedina Zavec, A.; Benmoussa, A.; Berardi, A. C.; Bergese, P.; Bielska, E.; Blenkiron, C.; Bobis-Wozowicz, S.; Boilard, E.; Boireau, W.; Bongiovanni, A.; Borràs, F. E.; Bosch, S.; Boulanger, C. M.; Breakefield, X.; Breglio, A. M.; Brennan, M. Á.; Brigstock, D. R.; Brisson, A.; Broekman, M. L. D. L.; Bromberg, J. F.; Bryl-Górecka, P.; Buch, S.; Buck, A. H.; Burger, D.; Busatto, S.; Buschmann, D.; Bussolati, B.; Buzás, E. I.; Byrd, J. B.; Camussi, G.; Carter, D. R. F. R.; Caruso, S.; Chamley, L. W.; Chang, Y.-T. T.; Chaudhuri, A. D.; Chen, C.; Chen, S.; Cheng, L.; Chin, A. R.; Clayton, A.;

Clerici, S. P.; Cocks, A.; Cocucci, E.; Coffey, R. J.; Cordeiro-da-Silva, A.; Couch, Y.; Coumans, F. A. A. W.; Coyle, B.; Crescitelli, R.; Criado, M. F.; D'Souza-Schorey, C.; Das, S.; de Candia, P.; de Santana, E. F.; de Wever, O.; del Portillo, H. A.; Demaret, T.; Deville, S.; Devitt, A.; Dhondt, B.; di Vizio, D.; Dieterich, L. C.; Dolo, V.; Dominguez Rubio, A. P.; Dominici, M.; Dourado, M. R.; Driedonks, T. A. A. P.; Duarte, F. v.; Duncan, H. M.; Eichenberger, R. M.; Ekström, K.; el Andaloussi, S.; Elie-Caille, C.; Erdbrügger, U.; Falcón-Pérez, J. M.; Fatima, F.; Fish, J. E.; Flores-Bellver, M.; Försönits, A.; Frelet-Barrand, A.; Fricke, F.; Fuhrmann, G.; Gabrielsson, S.; Gámez-Valero, A.; Gardiner, C.; Gärtner, K.; Gaudin, R.; Gho, Y. S.; Giebel, B.; Gilbert, C.; Gimona, M.; Giusti, I.; Goberdhan, D. C. I. C.; Görgens, A.; Gorski, S. M.; Greening, D. W.; Gross, J. C.; Gualerzi, A.; Gupta, G. N.; Gustafson, D.; Handberg, A.; Haraszti, R. A.; Harrison, P.; Hegyesi, H.; Hendrix, A.; Hill, A. F.; Hochberg, F. H.; Hoffmann, K. F.; Holder, B.; Holthofer, H.; Hosseinkhani, B.; Hu, G.; Huang, Y.; Huber, V.; Hunt, S.; Ibrahim, A. G.-E. E.; Ikezu, T.; Inal, J. M.; Isin, M.; Ivanova, A.; Jackson, H. K.; Jacobsen, S.; Jay, S. M.; Jayachandran, M.; Jenster, G.; Jiang, L.; Johnson, S. M.; Jones, J. C.; Jong, A.; Jovanovic-Talisman, T.; Jung, S.; Kalluri, R.; Kano, S. ichi; Kaur, S.; Kawamura, Y.; Keller, E. T.; Khamari, D.; Khomyakova, E.; Khvorova, A.; Kierulf, P.; Kim, K. P.; Kislinger, T.; Klingeborn, M.; Klinke, D. J.; Kornek, M.; Kosanović, M. M.; Kovács, Á. F.; Krämer-Albers, E.-M. M.; Krasemann, S.; Krause, M.; Kurochkin, I. v.; Kusuma, G. D.; Kuypers, S.; Laitinen, S.; Langevin, S. M.; Languino, L. R.; Lannigan, J.; Lässer, C.; Laurent, L. C.; Lavieu, G.; Lázaro-Ibáñez, E.; le Lay, S.; Lee, M.-S. S.; Lee, Y. X. F.; Lemos, D. S.; Lenassi, M.; Leszczynska, A.; Li, I. T. T. S.; Liao, K.; Libregts, S. F.; Ligeti, E.; Lim, R.; Lim, S. K.; Linē, A.; Linnemannstöns, K.; Llorente, A.; Lombard, C. A.; Lorenowicz, M. J.; Lörincz, Á. M.; Lötvall, J.; Lovett, J.; Lowry, M. C.; Loyer, X.; Lu, Q.; Lukomska, B.; Lunavat, T. R.; Maas, S. L. L. N.; Malhi, H.; Marcilla, A.; Mariani, J.; Mariscal, J.; Martens-Uzunova, E. S.; Martin-Jaular, L.; Martinez, M. C.; Martins, V. R.; Mathieu, M.; Mathivanan, S.; Maugeri, M.; McGinnis, L. K.; McVey, M. J.; Meckes, D. G.; Meehan, K. L.; Mertens, I.; Minciacchi, V. R.; Möller, A.; Møller Jørgensen, M.; Morales-Kastresana, A.; Morhayim, J.; Mullier, F.; Muraca, M.; Musante, L.; Mussack, V.; Muth, D. C.; Myburgh, K. H.; Najrana, T.; Nawaz, M.; Nazarenko, I.; Nejsum, P.; Neri, C.; Neri, T.; Nieuwland, R.; Nimrichter, L.; Nolan, J. P.; Nolte-'t Hoen, E. N. M. N.; Noren Hooten, N.; O'Driscoll, L.; O'Grady, T.; O'Loghlen, A.; Ochiya, T.; Olivier, M.; Ortiz, A.; Ortiz, L. A.; Osteikoetxea, X.; Ostegaard, O.; Ostrowski, M.; Park, J.; Pegtel, D. M.; Peinado, H.; Perut, F.; Pfaffl, M. W.; Phinney, D. G.; Pieters, B. C. C. H.; Pink, R. C.; Pisetsky, D. S.; Pogge von Strandmann, E.; Polakovicova, I.; Poon, I. K. K. H.; Powell, B. H.; Prada, I.; Pulliam, L.; Quesenberry, P.; Radeghieri, A.; Raffai, R. L.; Raimondo, S.; Rak, J.; Ramirez, M. I.; Raposo, G.; Rayyan, M. S.; Regev-Rudzki, N.; Ricklefs, F. L.; Robbins, P. D.; Roberts, D. D.; Rodrigues, S. C.; Rohde, E.; Rome, S.; Rouschop, K. M. M. A.; Rughetti, A.; Russell, A. E.; Saá, P.; Sahoo, S.; Salas-Huenuleo, E.; Sánchez, C.; Saugstad, J. A.; Saul, M. J.; Schiffelers, R. M.; Schneider, R.; Schøyen, T. H.; Scott, A.; Shahaj, E.; Sharma, S.; Shatnyeva, O.; Shekari, F.; Shelke, G. V.; Shetty, A. K.; Shiba, K.; Siljander, P. R. M. R.-M.; Silva, A. M.; Skowronek, A.; Snyder, O. L.; Soares, R. P.; Sódar, B. W.; Soekmadji, C.; Sotillo, J.; Stahl, P. D.; Stoorvogel, W.; Stott, S. L.; Strasser, E. F.; Swift, S.; Tahara, H.; Tewari, M.; Timms, K.; Tiwari, S.; Tixeira, R.; Tkach, M.; Toh, W. S.; Tomasini, R.; Torrecilhas, A. C.; Tosar, J. P.; Toxavidis, V.; Urbanelli, L.; Vader, P.; van Balkom, B. W. M. W.; van der Grein, S. G.; van Deun, J.; van Herwijnen, M. J. C. J.; van Keuren-Jensen, K.; van Niel, G.; van Royen, M. E.; van Wijnen, A. J.; Vasconcelos, M. H.; Vechetti, I. J.; Veit, T. D.; Vella, L. J.; Velot, É.; Verweij, F. J.; Vestad, B.; Viñas, J. L.; Visnovitz, T.; Vukman, K. v.; Wahlgren, J.; Watson, D. C.; Wauben, M. H. H. M.; Weaver, A.; Webber, J. P.; Weber, V.; Wehman, A. M.; Weiss, D. J.; Welsh, J. A.; Wendt, S.; Wheelock, A. M.; Wiener, Z.; Witte, L.; Wolfram, J.; Xagorari, A.; Xander, P.; Xu, J.; Yan, X.; Yáñez-Mó, M.; Yin, H.; Yuana, Y.; Zappulli, V.; Zarubova, J.; Žėkas, V.; Zhang, J. ye; Zhao, Z.; Zheng, L.; Zheutlin, A. R.; Zickler, A. M.; Zimmermann, P.; Zivkovic, A. M.; Zocco, D.; Zuba-Surma, E. K.; Datta Chaudhuri, A.; de Candia, P.; de Santana, E. F.; de Wever, O.; del Portillo, H. A.; Demaret, T.; Deville, S.; Devitt, A.; Dhondt, B.; di Vizio, D.; Dieterich, L. C.; Dolo, V.; Dominguez Rubio, A. P.; Dominici, M.; Dourado, M. R.; Driedonks, T. A. A. P.; Duarte, F. v.; Duncan, H. M.; Eichenberger, R. M.; Ekström, K.; el Andaloussi, S.; Elie-Caille, C.; Erdbrügger, U.; Falcón-Pérez, J. M.; Fatima, F.; Fish, J. E.; Flores-Bellver, M.; Försönits, A.; Frelet-Barrand, A.; Fricke, F.; Fuhrmann, G.; Gabrielsson, S.; Gámez-Valero, A.; Gardiner, C.; Gärtner, K.; Gaudin, R.; Gho, Y. S.; Giebel, B.; Gilbert, C.; Gimona, M.; Giusti, I.; Goberdhan, D. C. I. C.; Görgens, A.; Gorski, S. M.; Greening, D. W.; Gross, J. C.; Gualerzi, A.; Gupta, G. N.; Gustafson, D.; Handberg, A.; Haraszti, R.

A.; Harrison, P.; Hegyesi, H.; Hendrix, A.; Hill, A. F.; Hochberg, F. H.; Hoffmann, K. F.; Holder, B.; Holthofer, H.; Hosseinkhani, B.; Hu, G.; Huang, Y.; Huber, V.; Hunt, S.; Ibrahim, A. G.-E. E.; Ikezu, T.; Inal, J. M.; Isin, M.; Ivanova, A.; Jackson, H. K.; Jacobsen, S.; Jay, S. M.; Jayachandran, M.; Jenster, G.; Jiang, L.; Johnson, S. M.; Jones, J. C.; Jong, A.; Jovanovic-Talisman, T.; Jung, S.; Kalluri, R.; Kano, S. ichi; Kaur, S.; Kawamura, Y.; Keller, E. T.; Khamari, D.; Khomyakova, E.; Khvorova, A.; Kierulf, P.; Kim, K. P.; Kislinger, T.; Klingeborn, M.; Klinke, D. J.; Kornek, M.; Kosanović, M. M.; Kovács, Á. F.; Krämer-Albers, E.-M. M.; Krasemann, S.; Krause, M.; Kurochkin, I. v.; Kusuma, G. D.; Kuypers, S.; Laitinen, S.; Langevin, S. M.; Languino, L. R.; Lannigan, J.; Lässer, C.; Laurent, L. C.; Lavieu, G.; Lázaro-Ibáñez, E.; le Lay, S.; Lee, M.-S. S.; Lee, Y. X. F.; Lemos, D. S.; Lenassi, M.; Leszczynska, A.; Li, I. T. T. S.; Liao, K.; Libregts, S. F.; Ligeti, E.; Lim, R.; Lim, S. K.; Linē, A.; Linnemannstöns, K.; Llorente, A.; Lombard, C. A.; Lorenowicz, M. J.; Lörincz, Á. M.; Lötvall, J.; Lovett, J.; Lowry, M. C.; Loyer, X.; Lu, Q.; Lukomska, B.; Lunavat, T. R.; Maas, S. L. L. N.; Malhi, H.; Marcilla, A.; Mariani, J.; Mariscal, J.; Martens-Uzunova, E. S.; Martin-Jaular, L.; Martinez, M. C.; Martins, V. R.; Mathieu, M.; Mathivanan, S.; Maugeri, M.; McGinnis, L. K.; McVey, M. J.; Meckes, D. G.; Meehan, K. L.; Mertens, I.; Minciacchi, V. R.; Möller, A.; Møller Jørgensen, M.; Morales-Kastresana, A.; Morhayim, J.; Mullier, F.; Muraca, M.; Musante, L.; Mussack, V.; Muth, D. C.; Myburgh, K. H.; Najrana, T.; Nawaz, M.; Nazarenko, I.; Nejsum, P.; Neri, C.; Neri, T.; Nieuwland, R.; Nimrichter, L.; Nolan, J. P.; Nolte-'t Hoen, E. N. M. N.; Noren Hooten, N.; O'Driscoll, L.; O'Grady, T.; O'Loghlen, A.; Ochiya, T.; Olivier, M.; Ortiz, A.; Ortiz, L. A.; Osteikoetxea, X.; Østergaard, O.; Ostrowski, M.; Park, J.; Pegtel, D. M.; Peinado, H.; Perut, F.; Pfaffl, M. W.; Phinney, D. G.; Pieters, B. C. C. H.; Pink, R. C.; Pisetsky, D. S.; Pogge von Strandmann, E.; Polakovicova, I.; Poon, I. K. K. H.; Powell, B. H.; Prada, I.; Pulliam, L.; Quesenberry, P.; Radeghieri, A.; Raffai, R. L.; Raimondo, S.; Rak, J.; Ramirez, M. I.; Raposo, G.; Rayyan, M. S.; Regev-Rudzki, N.; Ricklefs, F. L.; Robbins, P. D.; Roberts, D. D.; Rodrigues, S. C.; Rohde, E.; Rome, S.; Rouschop, K. M. M. A.; Rughetti, A.; Russell, A. E.; Saá, P.; Sahoo, S.; Salas-Huenuleo, E.; Sánchez, C.; Saugstad, J. A.; Saul, M. J.; Schiffelers, R. M.; Schneider, R.; Schøyen, T. H.; Scott, A.; Shahaj, E.; Sharma, S.; Shatnyeva, O.; Shekari, F.; Shelke, G. V.; Shetty, A. K.; Shiba, K.; Siljander, P. R. M. R.-M.; Silva, A. M.; Skowronek, A.; Snyder, O. L.; Soares, R. P.; Sódar, B. W.; Soekmadji, C.; Sotillo, J.; Stahl, P. D.; Stoorvogel, W.; Stott, S. L.; Strasser, E. F.; Swift, S.; Tahara, H.; Tewari, M.; Timms, K.; Tiwari, S.; Tixeira, R.; Tkach, M.; Toh, W. S.; Tomasini, R.; Torrecilhas, A. C.; Tosar, J. P.; Toxavidis, V.; Urbanelli, L.; Vader, P.; van Balkom, B. W. M. W.; van der Grein, S. G.; van Deun, J.; van Herwijnen, M. J. C. J.; van Keuren-Jensen, K.; van Niel, G.; van Royen, M. E.; van Wijnen, A. J.; Vasconcelos, M. H.; Vechetti, I. J.; Veit, T. D.; Vella, L. J.; Velot, É.; Verweij, F. J.; Vestad, B.; Viñas, J. L.; Visnovitz, T.; Vukman, K. v.; Wahlgren, J.; Watson, D. C.; Wauben, M. H. H. M.; Weaver, A.; Webber, J. P.; Weber, V.; Wehman, A. M.; Weiss, D. J.; Welsh, J. A.; Wendt, S.; Wheelock, A. M.; Wiener, Z.; Witte, L.; Wolfram, J.; Xagorari, A.; Xander, P.; Xu, J.; Yan, X.; Yáñez-Mó, M.; Yin, H.; Yuana, Y.; Zappulli, V.; Zarubova, J.; Žėkas, V.; Zhang, J. ye; Zhao, Z.; Zheng, L.; Zheutlin, A. R.; Zickler, A. M.; Zimmermann, P.; Zivkovic, A. M.; Zocco, D.; Zuba-Surma, E. K. Minimal Information for Studies of Extracellular Vesicles 2018 (MISEV2018): A Position Statement of the International Society for Extracellular Vesicles and Update of the MISEV2014 Guidelines. *Journal of Extracellular Vesicles* **2018**, *7* (1), 1535750. https://doi.org/10.1080/20013078.2018.1535750.

(7) Busatto, S.; Zendrini, A.; Radeghieri, A.; Paolini, L.; Romano, M.; Presta, M.; Bergese, P. The Nanostructured Secretome. *Biomaterials Science* **2020**, *8* (1), 39–63. https://doi.org/10.1039/C9BM01007F.

(8) Sódar, B. W.; Kittel, Á.; Pálóczi, K.; Vukman, K. v.; Osteikoetxea, X.; Szabó-Taylor, K.; Németh, A.; Sperlágh, B.; Baranyai, T.; Giricz, Z.; Wiener, Z.; Turiák, L.; Drahos, L.; Pállinger, É.; Vékey, K.; Ferdinandy, P.; Falus, A.; Buzás, E. I. Low-Density Lipoprotein Mimics Blood Plasma-Derived Exosomes and Microvesicles during Isolation and Detection. *Scientific Reports* **2016**. https://doi.org/10.1038/srep24316.

(9) Schulz, E.; Karagianni, A.; Koch, M.; Fuhrmann, G. Hot EVs – How Temperature Affects Extracellular Vesicles. *European Journal of Pharmaceutics and Biopharmaceutics* **2020**, *146*, 55–63. https://doi.org/10.1016/j.ejpb.2019.11.010.

(10) Osteikoetxea, X.; Sódar, B.; Németh, A.; Szabó-Taylor, K.; Pálóczi, K.; Vukman, K. v.; Tamási, V.; Balogh, A.; Kittel, Á.; Pállinger, É.; Buzás, E. I. Differential Detergent Sensitivity of Extracellular

Vesicle Subpopulations. *Organic and Biomolecular Chemistry* **2015**. https://doi.org/10.1039/c5ob01451d.

(11) Hong, C.-S.; Funk, S.; Muller, L.; Boyiadzis, M.; Whiteside, T. L. Isolation of Biologically Active and Morphologically Intact Exosomes from Plasma of Patients with Cancer. *Journal of Extracellular Vesicles* **2016**, *5* (1), 29289. https://doi.org/10.3402/jev.v5.29289.

(12) Lobb, R. J.; Becker, M.; Wen Wen, S.; Wong, C. S. F.; Wiegmans, A. P.; Leimgruber, A.; Möller, A. Optimized Exosome Isolation Protocol for Cell Culture Supernatant and Human Plasma. *Journal of Extracellular Vesicles* **2015**, *4* (1), 27031. https://doi.org/10.3402/jev.v4.27031.

(13) Zhang, X.; Borg, E. G. F.; Liaci, A. M.; Vos, H. R.; Stoorvogel, W. A Novel Three Step Protocol to Isolate Extracellular Vesicles from Plasma or Cell Culture Medium with Both High Yield and Purity. *Journal of Extracellular Vesicles* **2020**, *9* (1), 1791450. https://doi.org/10.1080/20013078.2020.1791450.

(14) Karimi, N.; Cvjetkovic, A.; Jang, S. C.; Crescitelli, R.; Hosseinpour Feizi, M. A.; Nieuwland, R.; Lötvall, J.; Lässer, C. Detailed Analysis of the Plasma Extracellular Vesicle Proteome after Separation from Lipoproteins. *Cellular and Molecular Life Sciences* **2018**. https://doi.org/10.1007/s00018-018-2773-4.

(15) Osteikoetxea, X.; Sódar, B.; Németh, A.; Szabó-Taylor, K.; Pálóczi, K.; Vukman, K. v.; Tamási, V.; Balogh, A.; Kittel, Á.; Pállinger, É.; Buzás, E. I. Differential Detergent Sensitivity of Extracellular Vesicle Subpopulations. *Organic & Biomolecular Chemistry* **2015**, *13* (38), 9775–9782. https://doi.org/10.1039/C5OB01451D.

(16) Ridolfi, A.; Brucale, M.; Montis, C.; Caselli, L.; Paolini, L.; Borup, A.; Boysen, A. T.; Loria, F.; van Herwijnen, M. J. C.; Kleinjan, M.; Nejsum, P.; Zarovni, N.; Wauben, M. H. M.; Berti, D.; Bergese, P.; Valle, F. AFM-Based High-Throughput Nanomechanical Screening of Single Extracellular Vesicles. *Analytical Chemistry* **2020**, *92* (15), 10274–10282. https://doi.org/10.1021/acs.analchem.9b05716.

(17) RIDOLFI, A.; CASELLI, L.; MONTIS, C.; MANGIAPIA, G.; BERTI, D.; BRUCALE, M.; VALLE, F. Gold Nanoparticles Interacting with Synthetic Lipid Rafts: An AFM Investigation. *Journal of Microscopy* **2020**, *280* (3), 194–203. https://doi.org/10.1111/jmi.12910.

(18) Rikkert, L. G.; Nieuwland, R.; Terstappen, L. W. M. M.; Coumans, F. A. W. Quality of Extracellular Vesicle Images by Transmission Electron Microscopy Is Operator and Protocol Dependent. *Journal of Extracellular Vesicles* **2019**, *8* (1), 1555419. https://doi.org/10.1080/20013078.2018.1555419.

(19) Jørgensen, M.; Bæk, R.; Pedersen, S.; Søndergaard, E. K. L. L.; Kristensen, S. R.; Varming, K. Extracellular Vesicle (EV) Array: Microarray Capturing of Exosomes and Other Extracellular Vesicles for Multiplexed Phenotyping. *Journal of Extracellular Vesicles* **2013**, *2* (1), 20920. https://doi.org/10.3402/jev.v2i0.20920.

(20) Gori, A.; Romanato, A.; Greta, B.; Strada, A.; Gagni, P.; Frigerio, R.; Brambilla, D.; Vago, R.; Galbiati, S.; Picciolini, S.; Bedoni, M.; Daaboul, G. G.; Chiari, M.; Cretich, M. Membrane-Binding Peptides for Extracellular Vesicles on-Chip Analysis. *Journal of Extracellular Vesicles* **2020**. https://doi.org/10.1080/20013078.2020.1751428.

(21) Cretich, M.; di Carlo, G.; Longhi, R.; Gotti, C.; Spinella, N.; Coffa, S.; Galati, C.; Renna, L.; Chiari, M. High Sensitivity Protein Assays on Microarray Silicon Slides. *Analytical Chemistry* **2009**, *81* (13), 5197–5203. https://doi.org/10.1021/ac900658c.

(22) Cretich, M.; Bagnati, M.; Damin, F.; Sola, L.; Chiari, M. Overcoming Mass Transport Limitations to Achieve Femtomolar Detection Limits on Silicon Protein Microarrays. *Analytical Biochemistry* **2011**, *418* (1), 164–166. https://doi.org/10.1016/j.ab.2011.07.004.

(23) Michell, D. L.; Vickers, K. C. Lipoprotein Carriers of MicroRNAs. *Biochimica et Biophysica Acta (BBA) - Molecular and Cell Biology of Lipids* **2016**, *1861* (12), 2069–2074. https://doi.org/10.1016/j.bbalip.2016.01.011.

(24) Karlsen, T. A.; Aae, T. F.; Brinchmann, J. E. Robust Profiling of MicroRNAs and IsomiRs in Human Plasma Exosomes across 46 Individuals. *Scientific Reports* **2019**, *9* (1), 19999. https://doi.org/10.1038/s41598-019-56593-7.

(25) Axmann, M.; Meier, S.; Karner, A.; Strobl, W.; Stangl, H.; Plochberger, B. Serum and Lipoprotein Particle MiRNA Profile in Uremia Patients. *Genes* **2018**, *9* (11), 533. https://doi.org/10.3390/genes9110533.

(26) Weber, J. A.; Baxter, D. H.; Zhang, S.; Huang, D. Y.; Huang, K. H.; Lee, M. J.; Galas, D. J.; Wang, K. The MicroRNA Spectrum in 12 Body Fluids. *Clinical Chemistry* **2010**. https://doi.org/10.1373/clinchem.2010.147405.

(27) Borzi, C.; Calzolari, L.; Ferretti, A. M.; Caleca, L.; Pastorino, U.; Sozzi, G.; Fortunato, O. C-Myc Shuttled by Tumour-Derived Extracellular Vesicles Promotes Lung Bronchial Cell Proliferation through MiR-19b and MiR-92a. *Cell Death & Disease* **2019**, *10* (10), 759. https://doi.org/10.1038/s41419-019-2003-5.